Reduced dimensionality quantum scattering calculations on the $Cl+CH_4 \rightarrow HCl+CH_3$ reaction

Gunnar Nyman and Hua-Gen Yu
Department of Chemistry, Physical Chemistry, Göteborg University, S-412 96 Göteborg, Sweden

Robert B. Walker
Theoretical Division, Los Alamos National Laboratory, Los Alamos, New Mexico 87545

(Received 2 June 1998; accepted 6 July 1998)

Reduced dimensionality quantum scattering calculations using the Rotating Line Approximation, RLA, are performed on the $Cl+CH_4 \rightarrow HCl+CH_3$ reaction, treating CH_4 as a pseudo-diatom QH. A LEPS potential energy surface is used, where the zero-point energy of the modes not explicitly treated in the RLA calculations are included. The calculations are performed using hyperspherical coordinates and the improved log-derivative method of Manolopoulos. Boundary conditions have been applied using a hyperspherical projection method and an approximate method where the boundary conditions are applied directly in the hyperspherical coordinates. It is explicitly shown that the agreement between the methods is good. Scattering resonances are observed and related to the shape of the hyperspherical adiabats. Cumulative and state-to-state reaction probabilities are also presented. Vibrational adiabaticity is found to dominate without being exclusive. For $Cl+CH_4(v=1) \rightarrow HCl(n=1)+CH_3$ and a translational energy of 0.159 eV, measured differential cross sections give predominantly forward scattering, while for $Cl+CH_4(v=1) \rightarrow HCl(n=0)+CH_3$ there is predominantly backward and sideways scattering. Our calculated differential cross sections are in agreement with these general observations. Thermal rate constants have been calculated for the temperature range 200–800 K. The calculated rate constants are smaller than the experimental ones by less than 40% over the entire temperature range. © *1998 American Institute of Physics.* [S0021-9606(98)01038-1]

I. INTRODUCTION

The reaction of chlorine atoms with methane,

$$Cl(^2P)+CH_4 \rightarrow HCl+CH_3,$$

removes methane from the atmosphere and it also removes chlorine atoms, which can otherwise catalytically participate in ozone destruction in the stratosphere. Accordingly this reaction has drawn substantial interest and has been studied both experimentally and theoretically. Experimentally there has been several measurements of the thermal rate constant for the forward reaction and its reverse.[1–16] Recently state-to-state differential cross sections[17–21] and product rotational alignment[22] have been measured.[23] Theoretically the transition state has been characterized and the barrier height and vibrational frequencies have been calculated.[24–27] Gonzalez-Lafont *et al.* studied tunneling contributions to the reaction,[28] Duncan and Truong performed a direct *ab initio* dynamics study to calculate thermal and vibrationally state-selected rate constants within the canonical variational transition state theory formalism[27] and Espinosa-Garcia and Corchado constructed an analytic potential energy surface on which they studied kinetic isotope effects using variational transition state theory.[29] A classical trajectory study has also been performed to investigate several details of the reaction.[30]

In the classical trajectory study by Wang, Ben-Nun, and Levine[30] it was found that the essential features of the dynamics are not sensitive to the level of the detail with which the CH_3 radical is described. This was found by comparing results where CH_4 is modeled as a pseudo-diatom, $H-'CH_3'$, with full-dimensional calculations and with computations where CH_4 was treated as a triatomic, $H-C-'H_3'$. This observation provides incentive to perform a reduced dimensionality quantum mechanically based study of the $Cl+CH_4$ reaction.

In recent years there has been a growing interest in applying quantum dynamical methods to chemical reactions involving polyatomic molecules. A large number of calculations on four-atom reactions have been performed with focus on $H_2+OH \rightarrow H+H_2O$, see Refs. 31–34 and references therein. A small number of reactions involving more than four atoms have also been studied using quantum scattering techniques. For such reactions reduced dimensionality techniques are used. These reactions include $OH+CH_4 \rightarrow H_2O+CH_3$,[35,36] $H+C_2H_2 \rightarrow H_2+C_2H$,[37] $NH_3+OH \rightarrow NH_2+H_2O$,[38] $H+CH_4 \rightarrow H_2+CH_3$,[39] $Cl^-+CH_3Cl \rightarrow ClCH_3+Cl^-$,[40] and $Cl^-+CH_3Br \rightarrow ClCH_3+Br^-$.[41]

In the present work we use a 2D quantum scattering model to calculate reaction probabilities, thermal and state-selected rate constants and differential cross sections for the $Cl+CH_4 \rightarrow HCl+CH_3$ reaction. The model is in essence the Rotating Linear Model (RLM) but it incorporates an adiabatic correction that differs from that used in the Bending Corrected Rotating Linear Model (BCRLM).[42,43] This model was previously used to study the $CH_4+OH \rightarrow CH_3+H_2O$ reaction and it was termed the Rotating Line Approximation (RLA).[44]

 © 1998 American Institute of Physics

Downloaded 18 Dec 2006 to 203.250.225.122. Redistribution subject to AIP license or copyright, see http://jcp.aip.org/jcp/copyright.jsp

In the RLA framework, the studied reaction is written

$$QH(v)+Cl\rightarrow Q+HCl(n),$$

where the quantum number v represents the H–Q vibration and the quantum number n represents the HCl vibration.

The potential energy surface used in the calculations is a London-Eyring-Polanyi-Sato (LEPS) function. It is constructed such that the zero-point energies of the modes not explicitly treated in the quantum dynamics calculations are accounted for in the potential function.

The remainder of this paper is structured such that in Sec. II the RLA calculations, the potential energy surface and some numerical aspects of the calculations are described. In Sec. III, primarily reaction probabilities, differential cross sections and thermal and state-selected rate constants are presented and discussed. Conclusions are offered in Sec. IV.

II. COMPUTATIONAL ASPECTS

A. The RLA calculations

In the RLA calculations, a Hamiltonian in two mathematical dimensions is used to describe the reaction $Cl+CH_4\rightarrow HCl+CH_3$. The physical motion of the coordinates treated occurs in a three-dimensional world. The CH_4 moiety is treated as a quasi-diatom QH, where Q is a quasi-atom with the mass of CH_3. In this way the $Cl+CH_4$ reaction is effectively reduced to a three-atom problem. The effect of the other atoms enters the scattering calculations only through adiabatic zero-point energy in the potential energy surface employed.

In hyperspherical coordinates the two-dimensional RLA Hamiltonian may be written[42]

$$\hat{H}=-\frac{\hbar^2}{2\mu\rho^3}\frac{\partial}{\partial\rho}\rho^3\frac{\partial}{\partial\rho}-\frac{\hbar^2}{2\mu\rho^2}\frac{\partial^2}{\partial\delta^2}+\frac{\hat{J}^2}{2\mu\rho^2}+V(\rho,\delta), \tag{1}$$

where

$$\mu=\left\{\frac{m_Q m_H m_{Cl}}{m_Q+m_H+m_{Cl}}\right\}^{1/2},\quad \rho=\sqrt{\frac{M_1R_1^2}{\mu}+\frac{M_2R_2^2}{\mu}},$$

$$\delta=\arctan\sqrt{\frac{M_2R_2^2}{M_1R_1^2}},$$

$$M_1=\frac{m_Q(m_{Cl}+m_H)}{m_Q+m_H+m_{Cl}}\ \text{and}\ M_2=\frac{m_{Cl}m_H}{m_{Cl}+m_H}.$$

Here $\hat{J}$ is the total angular momentum operator[42] associated with the rotation of Q-H-Cl as a rigid linear body. R_1 connects Q with the HCl center of mass. R_2 is the HCl internuclear separation. m_A is the mass of species A. ρ is the hyperradius and δ is the hyperangle. Other symbols have their usual meaning.

By setting $\Psi'=\rho^{-3/2}\Psi$, Eq. (1) can be transformed to

$$\hat{H}=-\frac{\hbar^2}{2\mu}\frac{\partial^2}{\partial\rho^2}-\frac{\hbar^2}{2\mu\rho^2}\frac{\partial^2}{\partial\delta^2}+\frac{\hbar^2}{2\mu\rho^2}\left[J(J+1)+\frac{3}{4}\right]+V(\rho,\delta), \tag{2}$$

where J is the total angular momentum quantum number.

The Hamiltonian can be written $\hat{H}=\hat{H}_\delta+\hat{H}_\rho$ where

$$\hat{H}_\delta=-\frac{\hbar^2}{2\mu\rho^2}\frac{\partial^2}{\partial\delta^2}+V(\delta;\rho_i), \tag{3}$$

and

$$\hat{H}_\rho=-\frac{\hbar^2}{2\mu}\left[\frac{\partial^2}{\partial\rho^2}-\frac{J(J+1)}{\rho^2}-\frac{3}{4\rho^2}\right]. \tag{4}$$

The index i on ρ indicates that ρ is divided into a number of sectors. $\hat{H}_\delta$ is diagonalized with a basis set of sine functions to give eigenvalues $E_k(\rho_i)$ and eigenvectors $H_k(\delta;\rho_i)$ in each sector.

For a fixed total energy E, chosen value of J and initial quantum state k', the total wave function is expanded in each sector i in the coupled channel form

$$\Psi_{k'}(\rho,\delta;\rho_i)=\sum_{k=1}^{N}h_{k'k}(\rho;\rho_i)H_k(\delta;\rho_i). \tag{5}$$

The coefficients $h_{k'k}$ in Eq. (5) are found by solving the coupled-channel equations, which in matrix form are[45]

$$\frac{d^2}{d\rho^2}\mathbf{h}(\rho;\rho_i)+\mathbf{D_H}(\rho_i)\mathbf{h}(\rho;\rho_i)=0, \tag{6}$$

where the diagonal matrix $\mathbf{D_H}(\rho_i)$ has elements

$$(D_H)_{k'k}(\rho_i)=\frac{2\mu}{\hbar^2}\left\{E-E_k(\rho_i)-\frac{3\hbar^2}{8\mu\rho_i^2}-\frac{\hbar^2J(J+1)}{2\mu\rho_i^2}\right\}\delta_{k'k}. \tag{7}$$

The coupled-channel equations are solved using the improved log-derivative method of Manolopolous.[46,47] Boundary conditions have been applied in two ways. First, an accurate approach requiring projections in hyperspherical coordinates, following Hayes, Pendergast and Walker[43] is employed. Second, an approximate approach where the boundary conditions are applied directly in hyperspherical coordinates is used.

In the hyperspherical projection approach, the wave function is asymptotically expanded as

$$\Psi_{k'}(R,r)=\sum_{k=1}^{N}f_{k'k}(R)F_k(r), \tag{8}$$

for a given J. R and r are Jacobi coordinates for the product or reactant arrangements and $F_k(r)$ are solutions to

$$\left[-\frac{\hbar^2}{2\mu}\frac{\partial^2}{\partial r^2}+V_F(r)-\epsilon_k\right]F_k(r)=0, \tag{9}$$

where $V_F(r)$ is the fragment potential as R becomes large. The asymptotic form of $f_{k'k}(R)$ can be written

$$f_{k'k}(R)\sim-i\lambda_k^{-1/2}\{\hat{h}_J^{(2)}(\lambda_kR)\delta_{k'k}-\hat{h}_J^{(1)}(\lambda_kR)S_{k'k}^J\}, \tag{10}$$

where $\hat{h}_J^{(i)}(\lambda_kR)$ are Ricatti-Hankel functions as defined by Calogero[48] and

Downloaded 18 Dec 2006 to 203.250.225.122. Redistribution subject to AIP license or copyright, see http://jcp.aip.org/jcp/copyright.jsp

$$\lambda_k^2=\frac{2\mu}{\hbar^2}\{E-\epsilon_k\}. \tag{11}$$

Proceeding as in Ref. 43, the S matrix can be obtained as

$$\mathbf{S}^J=-\boldsymbol{\lambda}^{1/2}\mathbf{W}^{-1}\mathbf{W}^*\boldsymbol{\lambda}^{-(1/2)}, \tag{12}$$

where $\boldsymbol{\lambda}$ is a diagonal matrix with elements $\lambda_{k'k}=\lambda_k\delta_{k'k}$ obtainable from Eq. (11) and

$$\mathbf{W}=(\mathbf{R}_4^{\rho_{\rm big}}\mathbf{X}^{(4)}-\mathbf{X}^{(2)})-i(\mathbf{R}_4^{\rho_{\rm big}}\mathbf{X}^{(3)}-\mathbf{X}^{(1)}). \tag{13}$$

Here $\rho_{\rm big}$ is a selected large value of ρ, $\mathbf{R}_4$ is a block of the $\mathbf{R}$ matrix,[43] here propagated to $\rho_{\rm big}$ and

$$X_{k'k}^{(1)}=\rho^{1/2}\int_0^{\delta_{\max}}H_{k'}(\delta;\rho_{\rm big})\hat{j}_J(\lambda_kR)F_k(r)d\delta, \tag{14}$$

$$X_{k'k}^{(2)}=\rho^{1/2}\int_0^{\delta_{\max}}H_{k'}(\delta;\rho_{\rm big})\hat{y}_J(\lambda_kR)F_k(r)d\delta, \tag{15}$$

$$X_{k'k}^{(3)}=\rho^{-(1/2)}\int_0^{\delta_{\max}}H_{k'}(\delta;\rho_{\rm big})[\lambda_kRF_k(r)\hat{j}'_J(\lambda_kR) +\{\tfrac{1}{2}F_k(r)+rF_k'(r)\}\hat{j}_J(\lambda_kR)]d\delta, \tag{16}$$

$$X_{k'k}^{(4)}=\rho^{-(1/2)}\int_0^{\delta_{\max}}H_{k'}(\delta;\rho_{\rm big})[\lambda_kRF_k(r)\hat{y}'_J(\lambda_kR) +\{\tfrac{1}{2}F_k(r)+rF_k'(r)\}\hat{y}_J(\lambda_kR)]d\delta, \tag{17}$$

where $\hat{j}$ and $\hat{y}$ are Ricatti Bessel functions and each of $X_{k'k}^{(i)}$ is a real number.

In the present work, the log-derivative method was used to propagate the wave function. Thus, Eq. (13) is rewritten in terms of the log-derivative matrix $\mathbf{Y}(\rho;\rho_i)=\mathbf{h}'(\rho;\rho_i)\times\mathbf{h}^{-1}(\rho;\rho_i)$. The result is

$$\mathbf{W}=(\mathbf{YX}^{(2)}-\mathbf{X}^{(4)})-i(\mathbf{YX}^{(1)}-\mathbf{X}^{(3)}), \tag{18}$$

and is evaluated for a large value of ρ.

In the approximate procedure, the boundary conditions

$$h_{k'k}(\rho;\rho_i)\sim\lambda_{k,i}^{-1/2}(\hat{h}_J^{(2)}(\lambda_{k,i}\rho)\delta_{k',k}-\hat{h}_J^{(1)}(\lambda_{k,i}\rho)S_{k'k,i}), \tag{19}$$

are applied when ρ is large, where

$$\lambda_{k,i}^2=\frac{2\mu}{\hbar^2}\left\{E-E_k(\rho_i)-\frac{3\hbar^2}{8\mu\rho_i^2}\right\}\delta_{k'k}. \tag{20}$$

The log derivative matrix is used to obtain the S matrix as

$$\mathbf{S^J}=[\mathbf{YO}-\mathbf{O}']^{-1}[\mathbf{YI}-\mathbf{I}'], \tag{21}$$

where the prime on $\mathbf{O}$ and $\mathbf{I}$ means differentiation with respect to ρ,

$$I_{k'k}(\rho)=\lambda_{k,i}^{-1/2}\hat{h}_J^{(2)}(\lambda_{k,i}\rho)\delta_{k'k} \tag{22}$$

and

$$O_{k'k}(\rho)=\lambda_{k,i}^{-1/2}\hat{h}_J^{(1)}(\lambda_{k,i}\rho)\delta_{k'k}. \tag{23}$$

The probability of going from an initial state (v), to a final state (n) is given by

$$P_{v\to n}^J=|S_{v\to n}^J|^2, \tag{24}$$

where $S_{v\to n}^J$ is an element of the S matrix. Cumulative reaction probabilities (CRPs) are obtained by summing the state-to-state reaction probabilities over all final and all initial states, in this case over n and v. To obtain ''total CRPs'' one must also sum over the quantum numbers not explicitly treated in a reduced dimensionality calculation.

Differential cross sections $\sigma_{v\to n}(\Theta)$ for going from an initial state v to a final state n are calculated using the relation

$$\sigma_{v\to n}(\Theta)=\frac{1}{4k_v^2}\left|\sum_J(2J+1)S_{v\to n}^JP_J(\cos(\Theta))\right|^2, \tag{25}$$

where

$$k_v^2=\frac{2\mu_r'}{\hbar^2}(E-E_v). \tag{26}$$

μ_r' is the reduced mass of the colliding system and E_v is the Cl+QH(v) energy. The reactive scattering angle θ_R is related to Θ by $\theta_R=\Theta-\pi$. $\theta_R=0$ corresponds to forward scattering and $\theta_R=\pi$ to backward scattering.

The thermal rate constant is calculated from[49,35]

$$k(T)=\frac{Q(T)Q_{\rm rot}^{\ddagger}(T)}{2\pi\hbar Q_r(T)}\int_{-\infty}^{+\infty}dE\ \exp\{-E/kT\}N(E,J=0), \tag{27}$$

where $Q(T)$ is the partition function at the transition state for all vibrational modes not treated explicitly in the RLA scattering calculations, $Q_{\rm rot}^{\ddagger}(T)$ is the rigid rotor symmetric top approximation for the rotational partition function of the CH_4Cl complex, $Q_r(T)$ is the reactant partition function per unit volume and $N(E,J=0)$ is the cumulative reaction probability evaluated for $J=0$ only and referred to the QH$(v=0)$ level.

State-selected rate constants, $k_v(T)$, are calculated for Cl+HQ$(v)\to$HCl+Q, i.e., they are resolved in the initial vibrational quantum number. The state-selected rate constants are obtained from

$$k_v(T)=\frac{Q(T)Q_{\rm rot}^{\ddagger}(T)}{2\pi\hbar Q_r'(T)}\times\int_{-\infty}^{+\infty}dE\ \exp\{-E/kT\}N_v(E-E_v,J=0), \tag{28}$$

where $Q_r'(T)$ is the reactant partition function per unit volume but excluding the contribution from the Q–H vibration. $N_v(E,J=0)$ is the cumulative reaction probability except that it is not summed over v.

The ground state tunneling coefficient, η^G, is defined as the ratio of the thermal rate constant out of the ground state to the thermal rate constant out of the ground state obtained if reaction probabilities below the vibrationally adiabatic threshold are set to zero.[35] Proceeding as in Ref. 35, η^G can be written

$$\eta^G=\frac{\int_{-\infty}^{+\infty}dE\ \exp\{-E/kT\}N_{v=0}(E,J=0)}{\int_{E^*}^{+\infty}dE\ \exp\{-E/kT\}N_{v=0}(E,J=0)}, \tag{29}$$

where E^* is the vibrationally adiabatic threshold energy.

Downloaded 18 Dec 2006 to 203.250.225.122. Redistribution subject to AIP license or copyright, see http://jcp.aip.org/jcp/copyright.jsp

TABLE I. LEPS Morse parameters used (atomic units). The Sato parameter is 0.1976.

	r_{QH}	r_{QCl}	r_{HCl}
r_e	2.06169[a]	3.38072[b]	2.4093[c]
D_e	0.171551[d]	0.135418[b]	0.1697[c]
β	1.00644[e]	0.919075[b]	0.989[c]

[a]For C-H bond in CH_4 (Ref. 66).
[b]For C-Cl bond in CH_3Cl (Ref. 67).
[c]From Ref. 68.
[d]For C-H bond in CH_4 adding zero point energy to spectroscopic dissociation energy (Ref. 66).
[e]Varied to give a QH frequency of 3118 cm^{-1}.

The transmission coefficient, κ^G, gives the ratio of the quantum mechanical ground state rate constant to the one where no tunneling occurs and there is no reflection at energies above the adiabatic ground state barrier.[50] This can be written[35]

$$\kappa^G=\frac{1}{kT}\exp\left\{\frac{E^*}{kT}\right\}\int_{-\infty}^{+\infty}dE\ \exp\{-E/kT\}N_{v=0}(E,J=0). \tag{30}$$

B. Potential energy surface

The potential energy surface is modeled by a LEPS function,[51] using the parameters given in Table I. The Sato parameter was varied so as to obtain a barrier height of 7.3 kcal/mol, which gives a vibrationally adiabatic ground state (VAG) barrier height of 3.5 kcal/mol when the harmonic zero point energies of the modes treated explicitly in the RLA calculations are added to the LEPS surface. The LEPS surface is 1.2 kcal/mol endoergic, which comes out to 1.0 kcal/mol endoergic when the harmonic zero point energies of the RLA treated modes are added. Truong and Truhlar obtained a VAG barrier height of 3.5 kcal/mol and an endoergicity of 1.2 kcal/mol in *ab initio* (MP-SAC2) calculations, using harmonic zero-point energies.[24] The present surface does not treat spin-orbit coupling.

The present surface gives a QH fundamental vibrational frequency of 2989 cm^{-1} with the RLA code. Normal mode analysis gives a QH frequency of 3118 cm^{-1}. The experimental value is 3019 cm^{-1} for the triply degenerate normal modes ν_{3b} of CH_4, where a CH stretch is identified,[52] while the *ab initio* calculated harmonic value is 3218 cm^{-1}.[24] The HCl fundamental vibrational frequency is calculated to be 2872 cm^{-1} with the RLA code, while normal mode analysis gives a harmonic frequency of 2991 cm^{-1}. This can be compared to 2885 cm^{-1} for the experimental fundamental frequency and 2991 cm^{-1} for the harmonic value.[53] The potential energy surface is illustrated in Fig. 1, where the QH and HCl internuclear distances are displayed for a collinear arrangement of QHCl. The collinear arrangement entails the minimum energy path from reactants to products.

C. Numerical aspects

In all RLA calculations employing the hyperspherical projection method, the log-derivative propagation has been initiated at a hyper-radius $\rho=6.5$ a.u. and terminated at $\rho=25$ a.u. and approximately 500 sectors were used. To check that the computer code is correctly implemented we have reproduced the $v=0\rightarrow v'=0$ transition probabilities[54] for the $H+H_2(v)\rightarrow H_2(v')+H$ reaction on the DMBE potential energy surface. Further, the calculations on $Cl+CH_4$ were performed both in Los Alamos and Göteborg using independently written codes and all results agree between these sets of calculations.

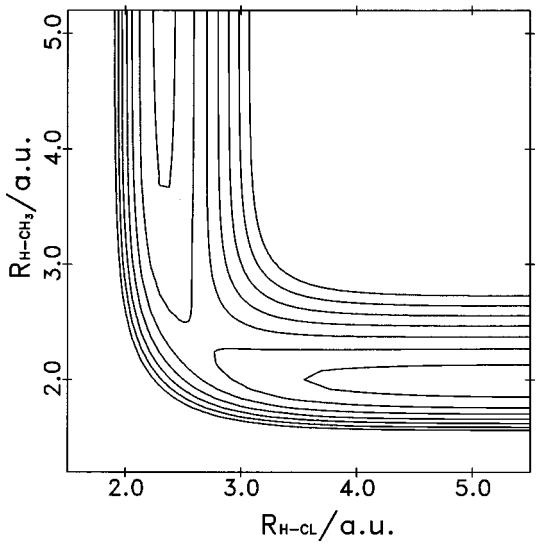

FIG. 1. 2D view of the potential energy surface for the $Cl+CH_4\rightleftharpoons CH_3+HCl$ reaction. The Cl–H–C angle is linear. The lowest potential curve is 2.306 kcal/mol above the minimum at large separations of the reactants. The interval between curves is 4.612 kcal/mol.

The Hamiltonian $\hat{H}_\delta$ in Eq. (3) was diagonalized using a basis set of 100 sine functions and employing a sine-DVR.[55] In Eqs. (5) and (8) we set $N=16$. Equation (9) was solved using 80 sine basis functions, employing a sine-DVR and diagonalizing the relevant matrix. $\mathbf{W}^{-1}$ in Eq. (12) was found using singular value decomposition.[56] Romberg integration or quadrature was used in solving Eqs. (14)–(17).

When using the approximate boundary conditions, the log-derivative propagation was initiated at $\rho=6.5$ a.u. and terminated at $\rho=35$ a.u. Approximately 750 sectors were used. The calculated reaction probabilities oscillate with sector[57,58] and the calculated probabilities were averaged over the last 100 sectors. All results shown in Sec. III were obtained with the hyperspherical projection method unless otherwise stated.

In order to evaluate the rate constants, the vibrational and rotational motions not treated in the RLA calculations are assumed separable. The rotational partition functions are evaluated by summing over the quantum mechanical energy levels of rigid rotors. The vibrational partition functions are evaluated in the quantum mechanical harmonic oscillator approximation.

Symmetry is not considered when evaluating the (external) rotational partition functions. Instead the rate constants are obtained from Eqs. (27), (28) by multiplying by a factor 4, which is obtained from the symmetry numbers 12, 1 and 3 for CH_4, Cl and the transition state respectively. The use of symmetry numbers results from assuming that nuclear spin is

Downloaded 18 Dec 2006 to 203.250.225.122. Redistribution subject to AIP license or copyright, see http://jcp.aip.org/jcp/copyright.jsp

separable from rotation, which has previously been found to be an excellent approximation when evaluating the rotational partition function of CH_4.[35]

In evaluating $Q^{\ddagger}_{\mathrm{rot}}(T)$, the symmetric top transition state moments of inertia were set to 3.431 amu Å^2 and 93.4(2) amu Å^2 based on an *ab initio* (MP-SAC2) determined geometry.[24] For the spherical top CH_4 reactant the moment of inertia was set to 3.15 amu Å^2. The vibrational frequencies at the transition state are in cm^{-1} 3118, 1227, 572, 3295 (2), 1441 (2), 874 (2), 324 (2) and 949*i*, while those for the CH_4 reactant are 3080, 1582 (2), 3218 (3) and 1364 (3).[24] The RLA calculations treat the symmetric stretch of the transition state complex. The corresponding frequency was taken to be 572 cm^{-1}, which is thus not included in $Q(T)$.

In evaluating electronic partition functions the four-fold degenerate ground state of chlorine ($^2P_{3/2}$) and the doubly degenerate ($^2P_{1/2}$) state, which is 882 cm^{-1} above the ground state, are included. For the transition state it is assumed that the lowest electronic state is doubly degenerate and that other states can be neglected. For CH_4 only the nondegenerate ground state is considered. Some further details on the evaluation of the thermal rate constant are given in Ref. 35.

III. RESULTS AND DISCUSSION

A. Hyperspherical adiabats

Much can be learned about a chemical reaction by studying the hyperspherical adiabats.[59] This is particularly true for a heavy-light-heavy system, which is due to the good separation of time scales between changes in ρ and in δ.

In Fig. 2, the hyperspherical adiabats from the RLA calculations are shown.

B. Reaction probabilities

Cumulative reaction probabilities $N(E,J=0)$ as a function of energy are shown in Fig. 3. The energy is referred to the bottom of the potential for the $Cl+CH_4$ reactants. The zero point energy of the reactants, as treated in the scattering calculations, is 0.1913 eV. The VAG barrier height is 0.15 eV. The first peak in the cumulative reaction probability is centered at 0.14 eV above the reactant zero point level and is solely due to transitions between the lowest reactant and product states as no other states are open.

There is a peak at 0.618 eV, which corresponds to reaction out of the $Cl+CH_4(v=1)$ state as it becomes open. There is also a peak at 0.934 eV, which corresponds to reaction out of the $Cl+CH_4(v=2)$ state as it becomes open.

There are spikes at 0.548, 0.819, 0.868, 0.906, 0.918, 1.11, 1.16, 1.20 and 1.24 eV. These are related to the energy eigenvalues found by diagonalizing the motion on the hyperspherical adiabats which are seen to have wells in Fig. 2. The lowest eigenvalues come out to be 0.543, 0.812, 0.861, 0.899, 1.10, 1.15, 1.19 and 1.23 eV. There is also an eigenvalue at 0.915 eV which corresponds to a state that is just barely unbound. The good agreement between the mentioned peaks and the energy eigenvalues relate to the time scale separation between the reactive H-atom motion, represented by the hyperangle δ, and the motion of the complex, represented by the hyper-radius ρ. This has been discussed in detail before by Römelt for several heavy-light-heavy reactions,[60–62] where it is also described how the agreement between the eigenvalues and the scattering resonances can be improved.

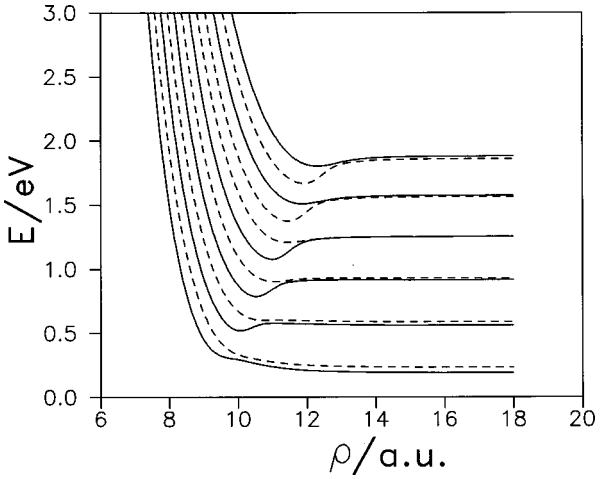

FIG. 2. Hyperspherical adiabatic energy levels for the $Cl+CH_4 \rightleftharpoons HCl+CH_3$ reaction as a function of the hyper-radius. Solid lines are for adiabats representing reactants at large values of the hyper-radius ρ, while dashed lines are for adiabats representing products at large values of ρ.

In Fig. 4 the total reaction probability out of $Cl+CH_4(v=0)$ is shown as a function of total angular momentum, J. For a total energy of 0.55 eV, a dip is seen at $J=8$. For $J=8$, 0.0017 eV of the energy is tied up in orbital rotation and 0.5483 eV remains, matching one of the spikes in Fig. 3. The solid lines are obtained by explicitly performing the RLA calculations for all values of J, while the dashed lines are obtained using the J-shift approximation.[63] It is noteworthy how well the spike at $J=8$ is picked up in the J-shift approximation. Tunneling occurs at energies below 0.34 eV (the energy is measured from the bottom of the potential well). We have previously found that the J-shift approximation is quite accurate in the tunneling regime for

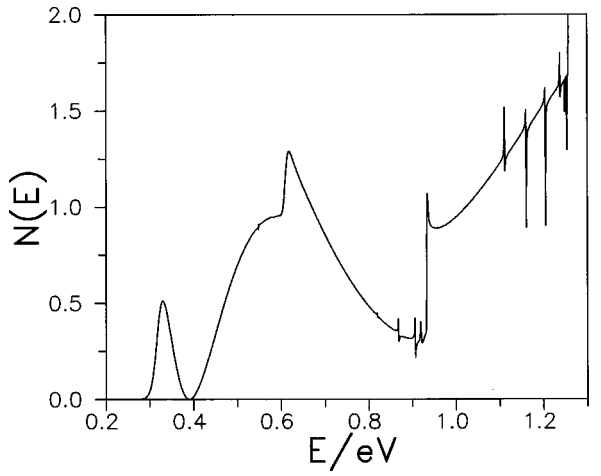

FIG. 3. Cumulative reaction probabilities vs total energy for $Cl+CH_4 \rightarrow HCl+CH_3$.

Downloaded 18 Dec 2006 to 203.250.225.122. Redistribution subject to AIP license or copyright, see http://jcp.aip.org/jcp/copyright.jsp

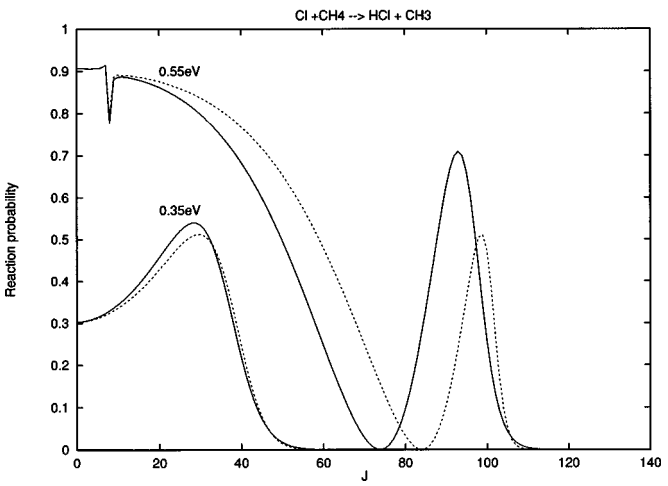

FIG. 4. Cumulative reaction probabilities vs total angular momentum for $Cl+CH_4 \rightarrow HCl+CH_3$. RLA results (solid lines) compared to J-shift results (dashed lines). The total energy is indicated.

the reactions $CH_4+OH \rightarrow CH_3+H_2O$ (Ref. 35) and $NH_3+OH \rightarrow NH_2+H_2O$.[38] This is found to agree also with the present calculations.

In Figs. 5, 6, 7 state-to-state reaction probabilities are shown. Note the different scales in the figures. From these figures it is seen that reaction out of $CH_4(v=0)$ preferentially forms $CH_3+HCl(n=0)$ and similarly for other initial states. While the vibrational adiabaticity dominates, it is not exclusive. The strong propensity for the vibrational quantum number to be conserved between reactants and products is not surprising as the reaction is close to thermoneutral and the vibrational frequencies are of similar magnitude. This behavior has been observed before, see, e.g., Ref. 64.

Panel B in Fig. 7 is included to illustrate the effect of using the approximate boundary conditions. It can be seen that the agreement with the corresponding results from the hyperspherical projection method in panel A is quite good.

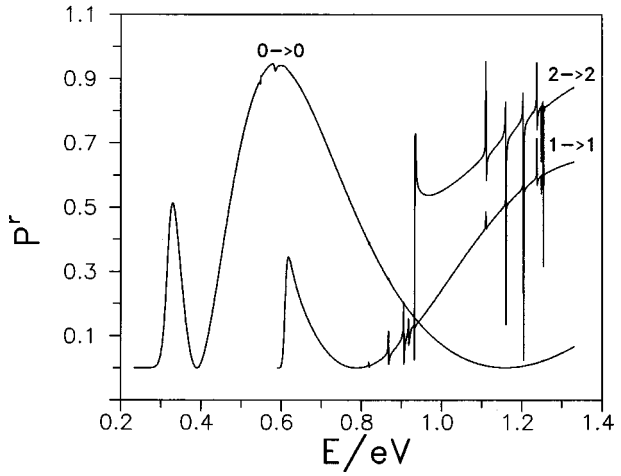

FIG. 5. State-to-state reaction probabilities vs total energy for $Cl+CH_4(v) \rightarrow HCl(n)+CH_3$ with $J=0$. The $v \rightarrow n$ transitions are indicated.

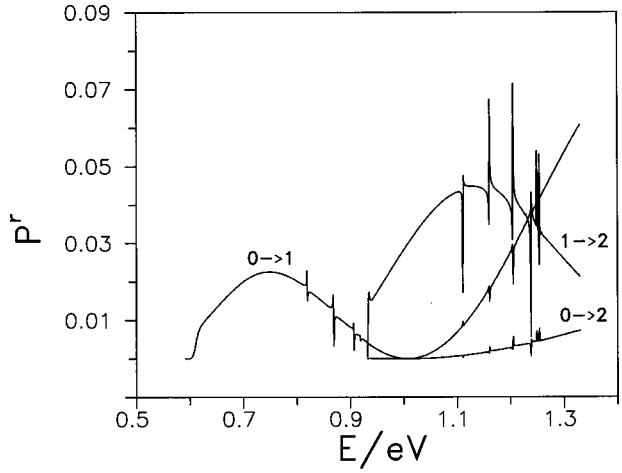

FIG. 6. State-to-state reaction probabilities vs total energy for $Cl+CH_4(v) \rightarrow HCl(n)+CH_3$ with $J=0$. The $v \rightarrow n$ transitions are indicated.

C. Differential cross sections

In Fig. 8, calculated state-to-state differential cross sections are shown for $Cl+CH_4(v=0) \rightarrow HCl(n=0)+CH_3$. Back and side scattering are seen to dominate at the lowest

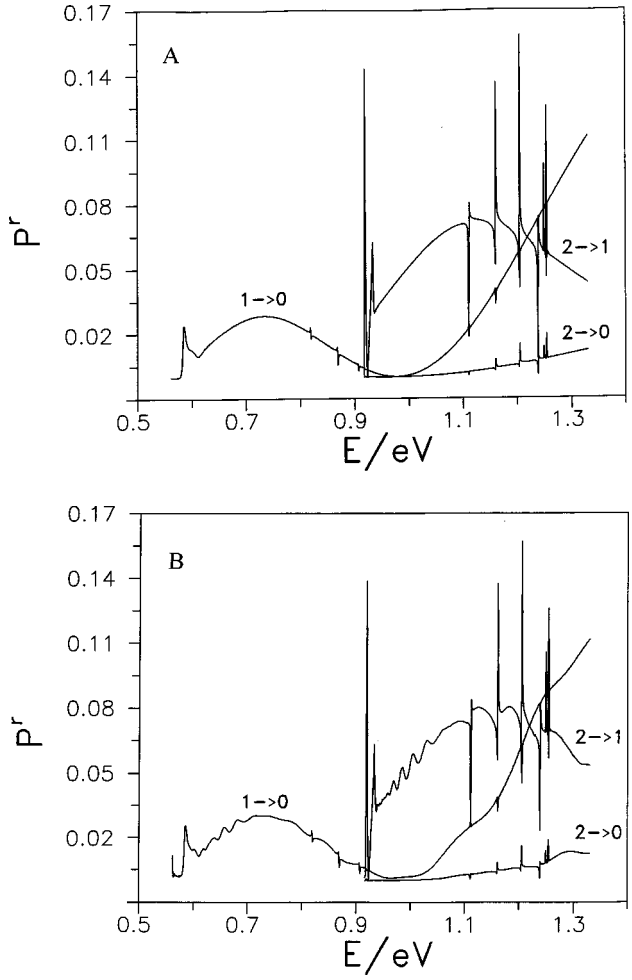

FIG. 7. State-to-state reaction probabilities vs total energy for $Cl+CH_4(v) \rightarrow HCl(n)+CH_3$ with $J=0$. The $v \rightarrow n$ transitions are indicated. The results in panel B were obtained using the approximate boundary conditions.

Downloaded 18 Dec 2006 to 203.250.225.122. Redistribution subject to AIP license or copyright, see http://jcp.aip.org/jcp/copyright.jsp

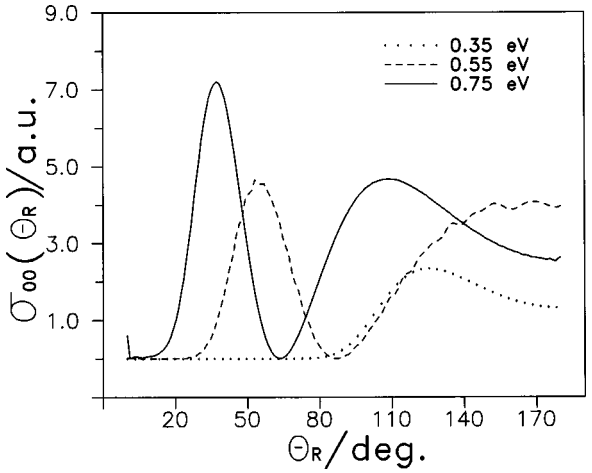

FIG. 8. State-to-state differential cross sections versus θ_R for $Cl+CH_4(v=0)\rightarrow HCl(n=0)+CH_3$. The total energy is indicated, of which 0.1913 eV is reactant zero point energy.

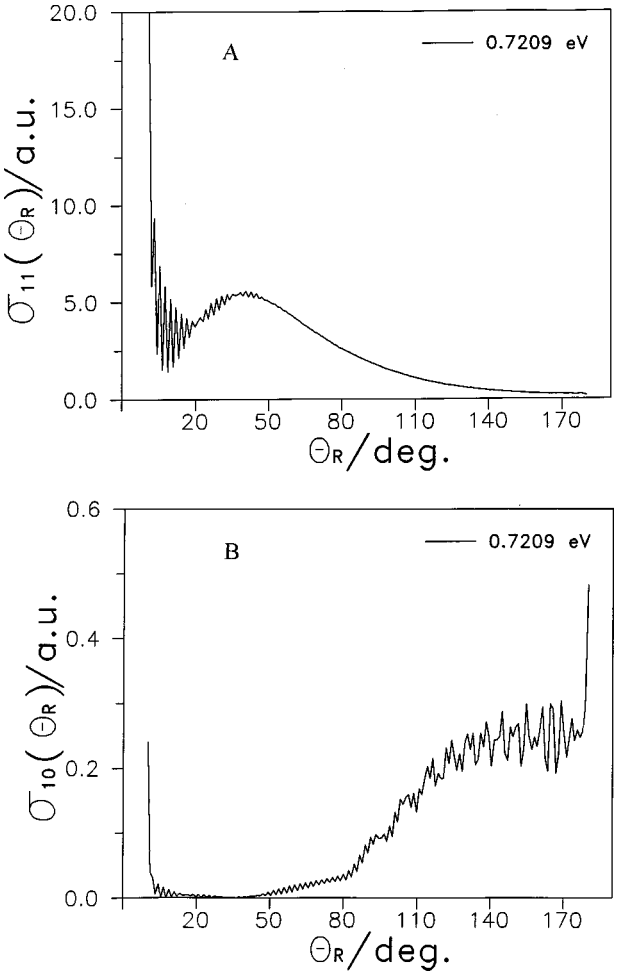

FIG. 9. State-to-state differential cross sections vs θ_R. The total energy is indicated, of which 0.159 eV is reactant translational energy. Panel A: $Cl+CH_4(v=1)\rightarrow HCl(n=1)+CH_3$. Panel B: $Cl+CH_4(v=1)\rightarrow HCl(n=0)+CH_3$.

energy. The higher the energy the larger the differential cross section and the more forward the scattering moves. This is expected as higher energies allow reaction to occur for larger angular momenta, i.e., for more peripheral collisions.

Calculated differential cross sections for going from $Cl+CH_4(v=1)\rightarrow HCl(n=1)+CH_3$ are shown in panel A of Fig. 9 for a translational energy of 0.159 eV. Experimentally, differential cross sections have been measured for $Cl+CH_4(v_3=1)\rightarrow HCl(n=1,j)+CH_3$ at an average translational energy of 0.159 eV.[19] The measured differential cross sections depend noticeably on the HCl rotational quantum number j. For $j=0,1,2$ forward scattering is more pronounced than backward scattering while for $j=3$ there is a larger peak for backward scattering than for forward scattering. In the classical trajectory study by Wang and Levine,[30] a j dependence in the differential cross sections is also observed, in particular for their 3-atom model of the reaction.

In our calculations HCl does not rotate and comparison to the experimental results for $j=0$ is most relevant. There is qualitative agreement with the experimental results even though there are differences in detail, which may originate both from the approximate potential used and the approximations invoked in the dynamics calculations.

Calculated differential cross sections for going from $Cl+CH_4(v=1)\rightarrow HCl(n=0)+CH_3$ are shown in panel B of Fig. 9 for a translational energy of 0.159 eV. The scattering is seen to be predominantly back and side scattered. This is in qualitative agreement with the experimental results, which for the reported product states ($n=0$, $j=3,5,6,8$) are predominantly scattered in the backward hemisphere. There is not an obvious forward/backward correlation to j, for the experimental $v=1\rightarrow n=0$ differential cross sections.

In producing the experimental differential cross section some uncertainty arises from the fact that it is not fully known to what extent the methyl fragment is vibrationally excited.[19] We hope to extend our calculation to include the methyl umbrella motion, which could help to resolve this issue.

D. Thermal rate constant and tunneling

In Fig. 10 the logarithm of the thermal rate constant for the CH_4+Cl reaction is shown vs inverse temperature. The experimental curves represents recent results of Pilgrim *et al.*[16] in the temperature range 292–800 K and Arrhenius fits to experimental data in the temperature range 200–500 K (Refs. 27, 65) are included together with the rate constants obtained in the RLA calculations. Rate constants obtained both with the hyperspherical projection method and using approximate boundary conditions are included, but they are so close that they cannot be distinguished.

The rate constants from the RLA calculations are approximately 35% smaller than the Arrhenius fits, while the deviations from the results of Pilgrim *et al.*[16] are smaller, but the slopes differ slightly here. Considering the simplifications made in the calculations and the approximate form of the potential, better agreement cannot be expected.

Ground state tunneling and transmission coefficients are shown in Table II. The ratio between the tunneling and transmission coefficients, η^G/κ^G, gives the recrossing for reaction out of the ground state, which is quite large. The re-

Downloaded 18 Dec 2006 to 203.250.225.122. Redistribution subject to AIP license or copyright, see http://jcp.aip.org/jcp/copyright.jsp

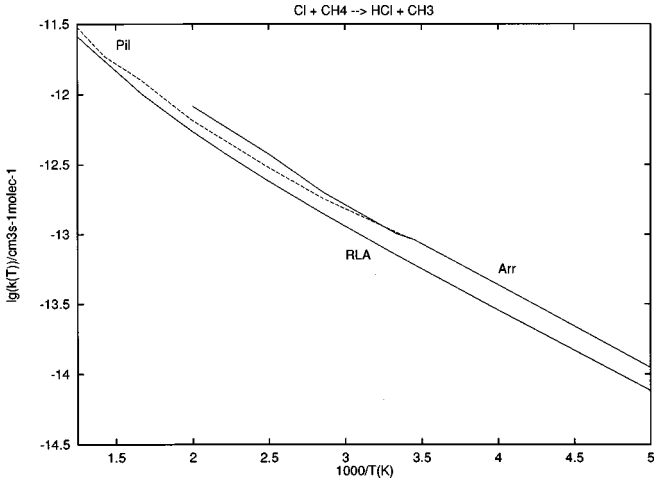

FIG. 10. The logarithm of the thermal rate constant versus inverse temperature for $Cl+CH_4 \rightarrow HCl+CH_3$. Results from the RLA calculations and experimental results by Pilgrim *et al.* (Ref. 16) (labeled ''Pil'') and from Ref. 27 (labeled ''Arr'') are included.

crossing partly balances the effect of tunneling on the rate constant.

In Table III thermal and state-selected rate constants are shown. It is seen that $k(T)$ and $k_{v=0}(T)$ are very close in values. $k_{v=1}(T=300\ \mathrm{K})$, however, is enhanced by more than an order of magnitude compared to $k_{v=0}(T=300\ \mathrm{K})$ and the difference should be experimentally detectable. The enhancement obtained here is, however, much smaller than the factor of about 300 obtained by Duncan and Truong.[27]

IV. CONCLUSIONS

Reduced dimensionality quantum scattering calculations using the Rotating Line Approximation (RLA), have been performed on the $Cl+CH_4 \rightarrow HCl+CH_3$ reaction. CH_4 is treated as a pseudo-diatom QH and the scattering calculations were restricted to collinear geometries. *Ab initio* calculations yields a linear transition state, which suggests that collinear geometries may dominate the reaction. A LEPS potential energy surface was used, where the zero-point energy of the modes not explicitly treated in the RLA calculations, have been included. The potential gives a vibrationally adiabatic ground state barrier height of 3.5 kcal/mol, which is in agreement with results from *ab initio* calculations.[24] Bearing in mind the simplifications made in treating the $Cl+CH_4$ reaction some encouraging results have been obtained.

TABLE II. Ground state tunneling and transmission coefficients.

T/K	η^G	κ^G
200.00	14.220	3.154
250.00	9.765	1.970
290.00	7.870	1.508
298.00	7.579	1.441
300.00	7.509	1.425
350.00	6.096	1.122
400.00	5.101	0.936
450.00	4.356	0.812
500.00	3.780	0.727

TABLE III. Thermal and state-selected rate constants for the $Cl+CH_4(v) \rightarrow HCl+CH_3$ reaction ($cm^3\ s^{-1}$).

T/K	$k(T)$	$k_{v=0}(T)$	$k_{v=1}(T)$
200	0.7616(−14)[a]	0.7615(−14)	0.3288(−12)
250	0.2851(−13)	0.2851(−13)	0.5644(−12)
290	0.6044(−13)	0.6044(−13)	0.7747(−12)
300	0.7091(−13)	0.7091(−13)	0.8299(−12)
350	0.1399(−12)	0.1399(−12)	0.1119(−11)
400	0.2393(−12)	0.2393(−12)	0.1430(−11)
450	0.3726(−12)	0.3725(−12)	0.1760(−11)
500	0.5434(−12)	0.5430(−12)	0.2108(−11)
600	0.1013(−11)	0.1012(−11)	0.2854(−11)
800	0.2588(−11)	0.2573(−11)	0.4518(−11)

[a]Power of 10 in parentheses. Four digits are shown to make visible the small difference between $k(T)$ and $k_{v=0}(T)$.

The calculations are performed using hyperspherical coordinates and the improved log-derivative method of Manolopoulos.[46,47] Boundary conditions have been applied using a hyperspherical projection method and an approximate method where the boundary conditions are applied directly in the hyperspherical coordinates. It is explicitly shown that the agreement between the methods is good for state-to-state reaction probabilities provided the approximate results are averaged over many sectors and that the propagation is continued to a comparatively large value of the hyperradius.

Scattering resonances were observed and related to the shape of the hyperspherical adiabats. Cumulative and state-to-state reaction probabilities were also presented. Vibrational adiabaticity was found to dominate without being exclusive.

State-to-state differential cross sections were calculated and compared to experimentally measured ones. For the $Cl+CH_4(v=1) \rightarrow HCl(n=1)+CH_3$ and a translational energy of 0.159 eV, the measured differential cross sections depend strongly on the HCl rotational state. For the ground rotational state, which corresponds closest to our calculations, the measurements give a predominantly forward scattering.[19] Our calculations are in agreement with this general observation even though there are differences in the details, which may be due to the potential energy surface and the approximations in the scattering model.

Measured state-to-state differential cross sections for the $Cl+CH_4(v=1) \rightarrow HCl(n=0)+CH_3$ reaction depend less on the rotational state of HCl and are predominantly back and side scattered for several rotational states and a translational energy of 0.159 eV.[19] Again, our calculated differential cross sections agree with the experimentally found dominance of scattering in the backward hemisphere.

Thermal rate constants have been calculated for the temperature range 200–800 K. The calculated rate constants are smaller than the experimental ones by less than 40% over the entire temperature range.

The experimental measurements suggest that the product CH_3 umbrella mode is mainly produced in the ground state. We intend to also investigate this theoretically as the experimentally derived differential cross sections depend on in which vibrational state(s) CH_3 is formed.

Downloaded 18 Dec 2006 to 203.250.225.122. Redistribution subject to AIP license or copyright, see http://jcp.aip.org/jcp/copyright.jsp

ACKNOWLEDGMENTS

This research was supported by the Swedish Natural Science Research Council. The calculations were carried out on a cluster of IBM workstations at Göteborg University. At Los Alamos, this work was performed under the auspices of the U.S. Department of Energy under the Laboratory Directed Research and Development Program. Calculations at Los Alamos were performed using HP workstations.

[1] M. A. A. Clyne and R. F. Walker, J. Chem. Soc., Faraday Trans. 1 **69**, 1547 (1973).
[2] C. L. Lin, M. T. Leu, and W. B. DeMore, J. Phys. Chem. **82**, 1772 (1978).
[3] R. Watson, G. Machado, S. Fischer, and D. D. Davis, J. Chem. Phys. **65**, 2126 (1976).
[4] R. G. Manning and M. J. Kurylo, J. Phys. Chem. **81**, 291 (1977).
[5] D. A. Whytock, J. H. Lee, J. V. Michael, W. A. Payne, and L. J. Stief, J. Chem. Phys. **66**, 2690 (1977).
[6] M. S. Zahniser, B. M. Berquist, and F. Kaufman, Int. J. Chem. Kinet. **10**, 15 (1978).
[7] L. F. Keyser, J. Chem. Phys. **69**, 214 (1978).
[8] M. H. Baghal-Vayjooee, A. J. Colussi, and S. W. Benson, J. Am. Chem. Soc. **100**, 3214 (1978).
[9] A. R. Ravishankara and P. H. Wine, J. Chem. Phys. **72**, 25 (1980).
[10] S. P. Heneghan, P. A. Knoot, and S. W. Benson, Int. J. Chem. Kinet. **13**, 677 (1981).
[11] J. P. Sawerysyn, C. Lafage, B. Meriaux, and A. Tighezza, J. Chim. Phys. **84**, 1187 (1987).
[12] O. Dobis and S. W. Benson, Int. J. Chem. Kinet. **19**, 691 (1987).
[13] J. J. Russel, J. A. Seetula, S. M. Senkan, and D. Gutman, Int. J. Chem. Kinet. **20**, 759 (1988).
[14] M.-L. Pohjonen and J. Koskikallio, Acta Chem. Scand. **33**, 449 (1979).
[15] P. Beichert, L. Wingen, J. Lee, R. Vogt, M. J. Ezell, M. Ragains, R. Neavyn, and B. J. Finlayson-Pitts, J. Phys. Chem. **99**, 13156 (1995).
[16] J. S. Pilgrim, A. McIlroy, and C. A. Taatjes, J. Phys. Chem. A **101**, 1873 (1997).
[17] W. R. Simpson, A. J. Orr-Ewing, and R. N. Zare, Chem. Phys. Lett. **212**, 163 (1993).
[18] W. R. Simpson, A. J. Orr-Ewing, T. P. Rakitzis, S. A. Kandel, and R. N. Zare, J. Chem. Phys. **103**, 7299 (1995).
[19] W. R. Simpson, T. P. Rakitzis, S. A. Kandel, A. J. Orr-Ewing, and R. N. Zare, J. Chem. Phys. **103**, 7313 (1995).
[20] W. R. Simpson, Ph.D. thesis, Stanford University, 1995.
[21] W. R. Simpson, T. P. Rakitzis, S. A. Kandel, T. Lev-On, and R. N. Zare, J. Phys. Chem. **100**, 7938 (1996).
[22] A. J. Orr-Ewing and R. N. Zare, Annu. Rev. Phys. Chem. **45**, 315 (1994).
[23] A. J. Orr-Ewing, W. R. Simpson, T. P. Rakitzis, S. A. Kandel, and R. N. Zare, J. Chem. Phys. **106**, 5961 (1997).
[24] T. N. Truong, D. G. Truhlar, K. K. Baldridge, M. S. Gordon, and R. Steckler, J. Chem. Phys. **90**, 7137 (1989).
[25] Y. Chen, A. Rauk, and E. Tschuikov-Roux, J. Phys. Chem. **95**, 9832 (1991).
[26] K. D. Dobbs and D. A. Dixon, J. Phys. Chem. **98**, 12584 (1994).
[27] W. T. Duncan and T. N. Truong, J. Chem. Phys. **103**, 9642 (1995).
[28] A. Gonzalez-Lafont, T. N. Truong, and D. G. Truhlar, J. Chem. Phys. **95**, 8875 (1991).
[29] J. Espinosa-Garcia and J. C. Corchado, J. Chem. Phys. **105**, 3517 (1996).
[30] X. Wang, M. Ben-Nun, and R. D. Levine, Chem. Phys. **197**, 1 (1995).
[31] S. K. Pogrebnya, J. C. Echave, and D. C. Clary, J. Chem. Phys. **107**, 8975 (1997).
[32] J. Z. H. Zhang, J. Dai, and W. Zhu, J. Phys. Chem. A **101**, 2746 (1997).
[33] W. Zhu, J. Z. H. Zhang, Y. C. Zhang, Y. B. Zhang, L. X. Zhan, S. L. Zhang, and D. H. Zhang, J. Chem. Phys. **108**, 3509 (1998).
[34] D. C. Clary, Science **279**, 1879 (1998).
[35] G. Nyman and D. C. Clary, J. Chem. Phys. **101**, 5756 (1994).
[36] G. Nyman, D. C. Clary, and R. D. Levine, Chem. Phys. **191**, 223 (1995).
[37] D. Wang and J. M. Bowman, J. Chem. Phys. **101**, 8646 (1994).
[38] G. Nyman, J. Chem. Phys. **104**, 6154 (1996).
[39] T. Takayanagi, J. Chem. Phys. **104**, 2237 (1996).
[40] D. C. Clary and J. Palma, J. Chem. Phys. **106**, 575 (1997).
[41] J.-L. L. Garrec, B. R. Rowe, J. L. Queffelec, J. B. A. Mitchell, and D. C. Clary, J. Chem. Phys. **107**, 1021 (1997).
[42] R. B. Walker and E. F. Hayes, in *The Theory of Chemical Reaction Dynamics*, edited by D. C. Clary (Reidel, Dordrecht, 1986), p. 105.
[43] E. F. Hayes, P. Pendergast, and R. B. Walker, in *Advances in Molecular Vibrations and Collision Dynamics: Reactive Scattering*, edited by J. M. Bowman (JAI, Greenwich, 1994), Vol. 2A.
[44] G. Nyman, Chem. Phys. Lett. **240**, 571 (1995).
[45] D. C. Clary, J. Chem. Phys. **95**, 7298 (1991).
[46] D. E. Manolopoulos, J. Chem. Phys. **85**, 6425 (1986).
[47] D. E. Manolopoulos, M. D'Mello, and R. E. Wyatt, J. Chem. Phys. **91**, 6096 (1989).
[48] F. Calogero, *Variable Phase Approach to Potential Scattering* (Academic, New York, 1967).
[49] U. Manthe, T. Seideman, and W. H. Miller, J. Chem. Phys. **99**, 10078 (1993).
[50] Y.-P. Liu, G. C. Lynch, T. N. Truong, D. H. Lu, D. G. Truhlar, and B. C. Garrett, J. Am. Chem. Soc. **115**, 2408 (1993).
[51] I. W. M. Smith, *Kinetics and Dynamics of Elementary Gas Reactions* (Butterworths, London, 1980).
[52] G. Herzberg, *Infrared and Raman Spectroscopy of Polyatomic Molecules* (Van Nostrand, New York, 1945).
[53] K. P. Huber and G. Herzberg, *Constants of Diatomic Molecules* (Van Nostrand, New York, 1979).
[54] J. Chang, N. J. Brown, M. D'Mello, R. E. Wyatt, and H. Rabitz, J. Chem. Phys. **97**, 6226 (1992).
[55] D. T. Colbert and W. H. Miller, J. Chem. Phys. **96**, 1982 (1992).
[56] W. H. Press, S. A. Teukolsky, W. T. Vetterling, and B. P. Flannery, *Numerical Recipes* (Cambridge University Press, Cambridge, 1986).
[57] G. Nyman and D. C. Clary, J. Chem. Phys. **99**, 7774 (1993).
[58] J. Römelt, Chem. Phys. Lett. **74**, 263 (1980).
[59] A. Ohsaki and H. Nakamura, Phys. Lett., C **187**, 1 (1990).
[60] J. Römelt, Chem. Phys. **79**, 197 (1983).
[61] J. Römelt and E. Pollak, in *Resonances in Electron-Molecule Scattering, van der Waals Complexes and Reactive Chemical Dynamics*, edited by D. G. Truhlar (American Chemical Society, Washington, D.C., 1984), p. 353.
[62] J. Römelt, in *The Theory of Chemical Reaction Dynamics*, edited by D. C. Clary (Reidel, Dordrecht, 1986), p. 77.
[63] J. M. Bowman, J. Phys. Chem. **95**, 4960 (1991).
[64] G. Nyman and D. C. Clary, J. Chem. Phys. **100**, 3556 (1994).
[65] W. B. DeMore, S. P. Sander, D. M. Golden, R. F. Hampson, M. J. Kurylo, C. J. Howard, A. R. Ravishankara, C. E. Kolb, and M. J. Molina, JPL publications 92-20, Jet Propulsion Laboratory, 1992.
[66] *CRC Handbook of Chemistry and Physics*, 62nd ed., edited by R. C. Weast (Chemical Rubber, Boca Raton, 1982).
[67] D. Wang and J. M. Bowman, J. Phys. Chem. **98**, 1608 (1994).
[68] D. C. Clary, G. Nyman, and R. Hernandez, J. Chem. Phys. **101**, 3704 (1994).

Downloaded 18 Dec 2006 to 203.250.225.122. Redistribution subject to AIP license or copyright, see http://jcp.aip.org/jcp/copyright.jsp